# Nanoscale

Accepted Manuscript


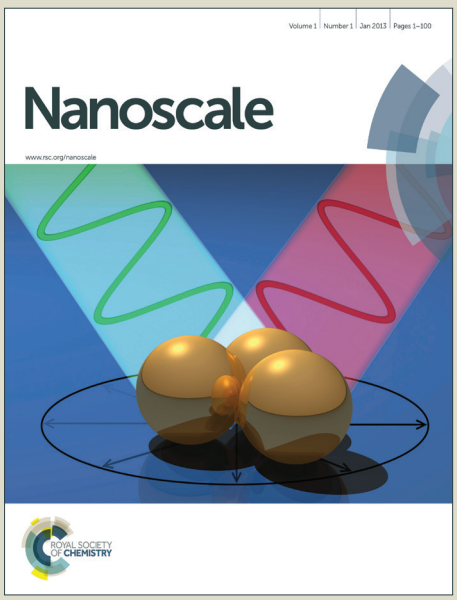





ROYAL SOCIETY OF CHEMISTRY

www.rsc.org/nanoscale

Nanoscale

RSCPublishing

ARTICLE

# Hybrid magnetic nanoparticle/nanogold cluster and its distance-dependent metal-enhanced fluorescence effect via DNA hybridization

Cite this: DOI: 10.1039/x0xx00000x

Received
Accepted

DOI: 10.1039/x0xx00000x

www.rsc.org/Nanoscale

Xuefan Gu† [a b], Youshen Wu† [a], Lingze Zhang [a], Yongchun Liu [a], Yan Li [a], Yongli Yan [b] and Daocheng Wu* [a]

To improve the metal-enhanced fluorescence (MEF) effect of nanogold (AuNPs) and accurately detect specific DNA sequences via DNA hybridization. A novel hybrid magnetic nanoparticle/nanogold cluster (HMNC) was designed based on finite-difference time-domain simulation results and prepared by using $Fe_3O_4$ and nanogolds. The nanogolds outside the HMNC were then conjugated with thiol-terminated DNA molecules, thus the DNA modified-HMNC (DNA-HMNC) was obtained. The size distributions of these nanostructures were measured by a Malvern size analyzer, and their morphology was observed via transmission electron microscopy (TEM). The ultraviolet (UV)–visible (vis) absorption spectra of the samples were recorded with a UV-2600 spectrophotometer. Fluorescence spectra and the MEF effect were obtained by a spectrophotofluorometer, and lifetimes were determined by a time-correlated single photon counting apparatus. The prepared HMNC was stable in aqueous solutions and had an average diameter of 87 ± 3.2 nm with six to eight AuNPs around a single $Fe_3O_4$ nanoparticle. Fluorescein isothiocyanate （FITC） tagged DNA-HMNC conjugates exhibited significant MEF effect and could accurately detect specific DNA sequences after DNA hybridization. This result indicates their various potential applications in sensors and biomedical fields.

## 1. Introduction

Gold nanoparticles or nanogolds (AuNPs) have attracted considerable attention because of their high physical and chemical stabilities in ambient conditions. In particular, AuNPs have unique size- and shape-dependent photophysical properties and localized surface plasmon resonances in the visible and near-infrared imbues[1, 2]. The surface of AuNPs can be modified and conjugated with a variety of biomacromolecules such as protein, polysaccharides, and polynucleotides. Therefore, AuNPs are widely applied in the fields of drug delivery, imaging, diagnostics, therapy biosensor devices, and other medical applications[3,4]. Among the photophysical detection methods of AuNPs, fluorescence detection is simple, fast, economical, and more sensitive to specific DNA sequences than other absorption detection methods. AuNPs do not fluoresced with sizes larger than 3 nm, but detecting analytes by using AuNPs based on fluorescence quenching has been realized[5,6]. DNA- functionalized AuNPs (DNA-AuNPs) have been recently used in a variety of forms to detect proteins[7, 8], oligonucleotides [9], metal ions [10], and other small molecules because of their high absorption coefficients and unique distance-dependent optical properties. Moreover, when hybridized to complementary DNA (cDNA) or associated particles, fluorophore-tagged DNA-AuNP (F-DNA-AuNP) nanosensors can exhibit extremely sharp fluorescence changes or quenching, which have been used to enhance the selectivity of detection target concentration in colorimetric format [11, 12]. For most reported F-DNA-AuNP nanosensors, AuNPs are used as efficient quenchers for fluorophores through energy transfer and electron transfer processes.

Nanoscale RSCPublishing

ARTICLE

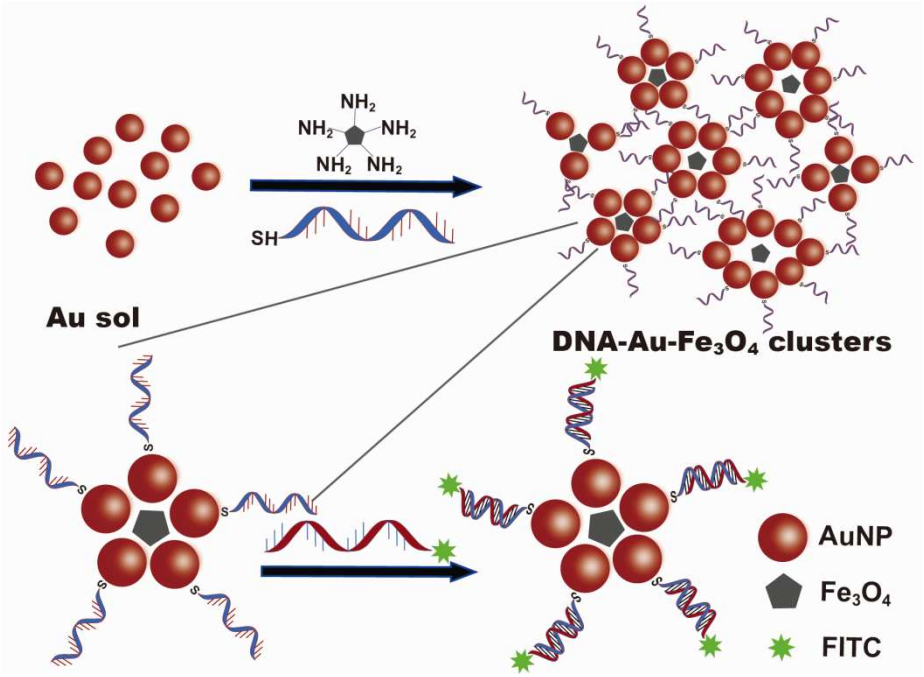


**Scheme.1** Schematic representation of the fabrication process of hybrid magnetic nanoparticle/nanogold cluster and their dye-tagged DNA modified conjugates.

AuNPs have higher quenching efficiencies than organic quencher molecules, which increases signal- signal- to-background ratio. Using AuNPs provide good sensitivity and a wide dynamic range for detecting target. However, some drawbacks of F-DNA-AuNPs, such as photobleaching rapidly, lower fluorescence quantum yields. In addition, instability in solutions needs to be overcome. The interaction between dye molecules and AuNPs is not limited to quenching. AuNP fluorophores are frequently quenched at a short distance from a metallic nanoparticle (gold, silver, or copper). But, the excitation and radioactive decay rates might be increased at a slight long distance, thus leading to increasing fluorescence intensity. This phenomenon is called metal-enhanced fluorescence (MEF) [13]. The MEF effect does not only increase the fluorescence intensity of a fluorophore, but also improves its photostability; moreover, MEF exhibits other desirable effects such as enhancing the fluorescence resonance energy transfer efficiency of two fluorophores [14, 15]. Given these promising features, the MEF effect has tremendous potential to address the drawbacks of F-DNA-AuNP detection. Miscellaneous studies have proven the effectiveness of the MEF effect of AuNPs. Spherical and rod-shaped AuNPs, as well as clusters of AuNPs, have been used in MEF studies and in enhancing MEF[16, 17]. Most MEF studies that involved AuNPs have been performed on planar substrates, which limit further applications of MEF in biological fields because most of the biological effects occur in solutions [18]. Chen *et al* [19] conducted a study on AuNP-enhanced fluorescent nanocomposites for solution-based MEF. The nanocomposite comprised an AuNP core, a thin PVP layer, a silica spacer shell of variable thicknesses, and a dye molecule-doped silica shell. They obtained a maximum fluorescence enhancement of approximately 9.2-fold. Capehart *et al*[20] also reported a nanocomposite with a 10 nm AuNP core and a spacer shell that was compromised with capsids and fluorophore-labeled DNA molecules of different lengths. They obtained a maximum fluorescent enhancement of 2.2-fold. Non-spherical AuNPs and clusters of AuNPs or AgNPs have also been used in studies on the MEF effect, and these nanostructures may provide higher enhancements than single spherical AuNP. Yuan

Nanoscale RSCPublishing

ARTICLE

*et al* [21] obtained high enhancements with chemically synthesized gold nanorods. However, the use of non-spherical gold nanostructures as EMF substrates in solution is rarely reported because of the difficult in fabrication NPs cluster with certain number of NPs and the instability of NP cluster aggregation owing to the same NPs. More recently, Schmidtke *et al* [22] developed a method to prepare hybrid NP clusters uses surface-modified of NPs core by a cross-linked poly(isoprene)-*b*-poly(ethylene glycol) diblock copolymer (PI-*b*-PEG) matrix and forms quasi-covalent Au–thiol with AuNPs around cross-linker NPs, thus leading to the formation of center-satellite type nanostructures with definite size and morphology. Furthermore, gold NPs or even closed gold shells were grown by *in situ* reductive deposition of $Au^{3+}$ ions on $Fe_2O_3$ NP seeds. This method provides an idea for preparing of hybrid NP cluster, but their MEF effects and theory simulation of related hybrid NP clusters have not been studied. Gill *et al* [23] used AgNP aggregates as MEF substrate in solutions. Considering that the inter-particle distances (termed "hotspots") of AgNP clusters ranged from 1 nm to 2 nm, large fluorescence enhancements were obtained. These previous study also pointed out that the quenching effect of a metallic surface may be overcome because the local enhancement of the electric field near hotspots is sufficiently large, and that the MEF effect can be realized even at a short distance. However, the method mentioned by Gill *et al* still exhibit uncontrolled NP numbers in clusters and instability in solutions because of the same NP modified the same property of functional group, the cluster aggregated easily and their MEF effects are uncertain in different time, thus limiting their applications in biological systems. If we fabricate hybrid AuNP clusters by using $Fe_3O_4$ NPs as the core and AuNPs as the shell (two of the NPs were modified with different property of functional groups), the NP numbers of the clusters around $Fe_3O_4$ NPs may be controlled by the size of the core and their interaction because of their different electrical properties. Moreover, the obtained hybrid AuNP/$Fe_3O_4$ NP cluster [hybrid magnetic nanoparticle/nanogold cluster (HMNC)] will be highly stable in solutions. By contrast, the local enhancement of the electric field effect in "hotspot" region for the same NP cluster is noteworthy. Several "hotspots" between NPs may disperse the entire electric field enhancement of the cluster, thus resulting in deficient fluorescent enhancement of the NP cluster. Hybrid NP thus clusters (such as HMNCs) receive less "hotspot" region electric field enhancement because of the different electrical properties of NPs, enhancing the electric field effect of the entire hybrid NP cluster. These phenomena have also been confirmed by our finite-difference time-domain (FDTD) simulation results and experimental investigation (Fig.1b, 1c, S1 and 5a). Based on the aforementioned investigation, we proposed a novel strategy to fabricate HMNC by using amino group-modified $Fe_3O_4$ NPs either as the core or as cross-linkers (Scheme 1). $Fe_3O_4$ NPs were initially synthesized and modified with amino groups on their surface, and the prepared $Fe_3O_4$@$NH_2$ NPs were added into the AuNP solution. HMNCs were then aggregated with a certain number of satellite AuNPs covering because of the size and strong interaction of the amino group with AuNPs. Finally, the surface of satellite AuNPs in the prepared HMNCs was conjugated with thiol-terminated DNA molecules; thus, DNA-modified HMNC (DNA-HMNC) were obtained. When the prepared DNA-HMNC conjugates were mixed with a certain length of complementary single-stranded DNA (ssDNA) tagged with fluorescein isothiocyanate (FITC) (F-DNA), significant fluorescence enhancement effect could be observed after DNA hybridization; thus, a specific DNA sequence could be accurately detected. This DNA-HMNC conjugate is stable in aqueous solutions and exhibits more significant fluorescent intensity enhancement than the corresponding F-DNA and AuNP clusters solution, thus indicating extensive possible applications in sensors and the biomedical fields.

## 2. Experimental Section

### 2.1. Materials

Gold(III) chloride trihydrate, trisodium citrate, nitric acid (65 wt%), 1,6-hexamethylene diamine, hydrochloric acid (HCl), and ethanol were purchased from the Sinopharm Chemical Reagent Co., Ltd. (Shanghai, China) and used as received. $Fe_3O_4$ nanoparticles (20 nm), (3-aminopropyl) trimethoxysilane (APTMS, 99%), and fluorescein isothiocyanate (FITC) were bought from Aladdin

Chemistry Co., Ltd (Shanghai, China). All other reagents were of analytical grade and used without further purification. Deionized water was used in all experiments. Alkanethiol ssDNA (SH-DNA) (5′ HS-C6-TAC CTG AAT GCG 3′, abbreviated as A1-S; 5′ TAC CTG AAT GCG-C6-SH 3′, abbreviated as A2-S ; 5′ HS-C6-CGGTGGCACA-CCTCGC 3′, abbreviated as C1-S; 5′ HS-C3-GGGGG-GGGGGGG-C3-Rhodamine B 3′, abbreviated as HS-G-R) and F-DNA (5′ FITC-CGC ATT CAG GTA 3′, abbreviated as F-B1; 5′ FITC-GGC ATT CAG GTA 3′, abbreviated as F-B2; 5′ FITC-C6-GCGAGGTGTGCCACCG 3′, abbreviated as F-D1; 5′GCGAGGTGTGCCACCG 3′, the 9th T is tagged with FITC, abbreviated as F-D2; 5′GCGAGGTGTGCCACCG-C6-FITC 3′, abbreviated as F-D3) purified via high-performance liquid chromatography were obtained from Sangon Biotech Co., Ltd. (Shanghai, China). DNA sequences were designed according to the following considerations. DNA should exhibit high potential to be used as a programmable nanoscaffold that allows positioning of nanoparticles or molecules in 3D [24]. Double-stranded DNA (dsDNA) is known to be rigid. It has a persistence length of approximately 50 nm in buffer solutions with low ionic strength, and its spacer length can be conveniently adjusted with 0.3 nm step size [25, 26]. Furthermore, SH-DNA molecules can be easily conjugated onto the surface of the Au film and the nanoparticles[27]. Thus, we designed the aforementioned DNA probes in this study.

### 2.2. Synthesizing AuNPs

AuNPs were synthesized according to the modified Turkevich method, which involves reverse addition. This method was conducted by adding $HAuCl_4$ to the citrate solution, thus producing monodispersed AuNPs [28, 29]. During typical AuNP fabrication, 200 mL of deionized water was heated to boiling point. Then, 4 mL of 1% trisodium citrate solution was immediately added into the boiling deionized water under constant stirring. Meanwhile, 4 mL of 1% $HAuCl_4$ was added and continually stirred for another 15 minutes. The obtained solution (0.096 mg/mL) was used as stock AuNP solution after it was cooled to room temperature.

### 2.3. Synthesizing functional silane-modified $Fe_3O_4$@$NH_2$ nanoparticles

Functional silane-modified $Fe_3O_4$ nanoparticles ($Fe_3O_4$@$NH_2$) were synthesized via a two-step process. In the first step, water-based ferrofluids were prepared by our previous method as follows [30]. Powdery $Fe_3O_4$ nanoparticles (8.0 g) were mixed with 0.3 mL of nitric acid and 400 mL deionized water. The mixture was ultrasonicated under stirring at 70 °C for 3h until the turbid suspension transformed into a homogeneous colloidal solution. Supernatant ferrofluids were obtained by centrifugation at 3000 rpm for 10 min. The final product of ferrofluids was concentrated to 8.0 mg/mL of $Fe_3O_4$ NP concentration by centrifugation at 8000 rpm. In the second step, 5.0 mL of the prepared water-based ferrofluids was added into 95 mL ethanol, pH was adjusted to 5.5, and 20 μL of APTMS was added into the mixture solution. The solution was incubated at 25 °C for 20 h, and the supernatant silane-modified $Fe_3O_4$@$NH_2$ NPs were obtained by centrifugation at 8000 rpm for 30 min. The precipitates were redispersed in HCl solution (pH 5.5) and diluted with 1% trisodium citrate solution to a final concentration of 1.0 mg $mL^{-1}$. This solution was passed through a membrane filter (0.22 μm pore size) and used as stock.

### 2.4. Synthesizing HMNCs and AuNP clusters

HMNCs were synthesized by adding $Fe_3O_4$@$NH_2$ NP solution into AuNP solution. Briefly, 15 μL of $Fe_3O_4$@$NH_2$ solution (1.0 mg $mL^{-1}$) was added into 4 mL of AuNP solution (0.096 mg $mL^{-1}$) under mild stirring for 30 min and passed through a membrane filter (0.45 μm pore size). AuNP clusters were synthesized by directly adding 1, 6-hexamethylene diamine (as cross-linker molecules) into AuNP solution. In a typical experiment, 35 μL of 1,6-hexamethylene diamine ($1 \times 10^{-3}$ mol $L^{-1}$ in water) was added into 5 mL of AuNP solution (0.096 mg $mL^{-1}$) under mild stirring for 30 min and passed through a membrane filter (0.45 μm pore size).

### 2.5. FDTD simulation

FDTD simulations were performed by using FDTD solution software (http://www.lumerical.com; Lumerical Solutions, Inc., Vancouver, Canada) [31]. Additional post-processing of FDTD data was performed via Microsoft Excel 2010 (Microsoft Corporation, Washington, USA). For our calculations, we used a grid size of 0.5 nm, a fixed excitation (incidence) wavelength of 488 nm, and water as the surrounding medium. The nanoparticle size was set to 20 nm, and the distance between each nanoparticle (for the seven nanoparticles) was approximately 1 nm.

### 2.6. Preparing DNA-AuNP and DNA-HMNC conjugates

SH-DNA was conjugated with AuNPs according to Mirkin's protocol [32, 33]. A total of 3 μL of A1-S ($5\times10^{-5}$ moL $L^{-1}$) was added

into 5 mL of AuNP solutions and mixed by mild stirring for 24 h. DNA-HMNC conjugates were prepared by following a similar process. A1-S (3 μL) or A2-S ($5\times10^{-5}$ moL $L^{-1}$) was added into 5 mL of HMNC solution and mixed by mild stirring for 24 h.

### 2.7. Preparing F-B1A1-S-HMNC and F-B1A2-S-HMNC conjugates

F-B1A1-S-HMNC and F-B1A2-S-HMNC conjugates were obtained by mixing the prepared ssDNA-S-HMNC conjugates with the same amount of F-B1 probes (which are complementary to the A1-S and A2-S molecules of the A1/A2-S-HMNC conjugates). Then, hybridization was carried out in 0.3 mol $L^{-1}$ PBS [containing 0.3 mol $L^{-1}$ NaCl, 9.5 mmol $L^{-1}$ phosphate buffer (pH 7)] solution for 2 h [32, 33]. To validate the hybridization efficiency of the prepared A1-S-HMNC, 0.3, 0.6, 0.9, 1.2, 1.5, 1.8, 2.1, 2.4, 2.7, and 3.0 μL of F-B1 probe solutions (50 μmol $L^{-1}$) were mixed and hybridized with a 5 mL solution of the prepared A1-S-HMNC conjugates, respectively. F-B1A1-S-AuNP conjugates were obtained by a similar process above.

### 2.8. Characterization

The morphologies of the nanostructure samples, such as AuNPs, $Fe_3O_4$NPs, DNA-AuNP clusters, HMNC clusters, and AuNP clusters without DNA, were observed via transmission electron microscopy (TEM) by using a JEM-3010 transmission electron microscope (JEOL Ltd., Tokyo, Japan) with a 300 kV electron source. Hydrodynamic diameter was measured with a Zetasizer Nano ZS90 (Malvern Instruments Ltd., Worcestershire, UK). The ultraviolet (UV)–visible (vis) absorption spectra of the previously mentioned samples were recorded with a UV-2600 spectrophotometer (Shimadzu Corporation, Kyoto, Japan). To investigate the stability of the prepared AuNP clusters and HMNC conjugates, the absorption spectra and hydrodynamic diameter of the prepared samples were regularly recorded for 1 month (every 5 days). To validate the conjugation of the SH-DNA and HMNC (and AuNPs), the prepared samples were mixed with NaCl solutions (0.15 mol $L^{-1}$ and 1 mol $L^{-1}$ respectively) and their absorption spectra were recorded.

The fluorescence spectra of F-B1A1-S-HMNC conjugates formed with different NPs or NP clusters were recorded in a solution by using a FluoroMax-4 fluorescence spectrophotometer (HORIBA Jobin Yvon, Kyoto, Japan). To investigate the effects of self-absorbance on the recorded fluorescence spectra of F-B1A1-S-HMNC3 conjugates, the prepared sample was exponentially diluted (1-, 2-, 4-, 8-, and 16-fold), and the fluorescence spectra were recorded. After our investigation, the fluorescence enhancement effect of A1-S-HMNC3 conjugates was also studied with a FluoroMax-4 fluorescence spectrophotometer. The fluorescence spectra of F-B1 and F-B1A1-S-HMNC3 conjugates at the same F-B1 concentration were recorded, and enhancement factors were determined by using the division of the maximum fluorescence intensity of the F-B1A1-S-HMNC3 conjugates and free F-B1.

The influences of surrounding factors such as temperature, pH values, and storage time for the fluorescence enhancement factor were investigated. Representative fluorescence lifetimes were measured by using a time-correlated single photon counting (44MXs-B, LeCroy, USA). The solution was excited with a fiber laser (SC400-4-PP, Fianium Ltd., Southampton, UK), and the result was recorded by a single photon counting apparatus (PicoHarp300, PicoQuant, Berlin, Germany). Data were analyzed by using multiple exponential models.

The melting temperature (*T*m) of the double strand DNA (dsDNA) is an important factor for DNA denaturation, which depends on the strand length, the specific nucleotide sequence of the DNA molecules and is strongly influenced by the ionic strength of the solution (salt concentration)[34]. According to the online oligonucleotide analyzer software (http://www.idtdna.com/), we calculated *T*m values of the current DNA sequence in this experiment with different salt concentrations. To determine the influence of pH values to the *T*m value, *T*m values of the DNA in different pH value solutions, such as pH 3.0 of buffer solutions (containing 300 mmol $L^{-1}$ NaCl and 1 mmol $L^{-1}$ HCl), pH 4.0 of buffer solution (containing 300 mmol $L^{-1}$NaCl and 0.1 mmol $L^{-1}$ HCl) and pH 7.0 of PBS buffer solution (containing 300 mmol $L^{-1}$ NaCl 1.5 m mol $L^{-1}$ $KH_2PO_4$ and 8.0 mmol $L^{-1}$ $K_2HPO_4$), have been measured as K Wilson and J walker described[35].

### 2.9. DNA hybridization detection

DNA hybridization detection assays were performed with F-dsDNA-HMNC conjugates prepared with different DNA probes. The conjugation of SH-DNA onto the HMNC conjugates were confirmed by the "salt solution test" and fluorescence determination[33,36]. Briefly, measurement of DNA conjugation was performed as follows: 30 μL of 1 μmol $L^{-1}$ DNA probe (5′ HS-C3-GGGGGGGGGGGG-C3-Rhodamine B

3′) solution was mixed with 5 mL of prepared HMNCs solution, and the mixture was gently stirred for 24 hours. The prepared conjugation solution was then separated by centrifugation for 40 min at 12000 rpm, and the supernatant was collected. By measuring the fluorescence emission intensity of the obtained supernatant, concentration of the remnant DNA probes in supernatant was then obtained. F-B1A1-S-HMNC3 conjugates were prepared with A1-S (5′ HS-C6-TAC CTGAAT GCG 3′)-tagged HNMC3s and F-B1 (5′ FITC-CGCATT CAGGTA 3′) probes. In F-B1A1-S-HMNC3 conjugates, FITC dyes were located at approximately 4 nm away from the surface of HMNCs, with 12 bp dsDNA as spacers. To investigate the influence of fluorophore-nanostructure distance on the MEF effect of F-dsDNA- HMNC conjugates, F-B1A2-S-HMNC3 conjugates were prepared with A2-S (5′ TAC CTGAATGCg-C6-SH 3′)-tagged HNMC3 and F-B1 (5′ FITC-CGCATT CAGGTA 3′) probes. In F-B1A2-S-HMNC3 conjugates, FITC dyes were located very near (less than 1 nm) to the surface of the HMNCs. Similarly, the MEF effect of other three F-dsDNA-HMNC conjugates, such as F-D1C1-S-HMNC conjugates (with fluorophore-nanostructure distance of about 5nm), F-D2C1-S-HMNC conjugates (with fluorophore-nanostructure distance of about 3nm) and F-D3C1-S-HMNC conjugates (in which the inter-distance are quite short) were investigated.

To investigate the influence of single mismatch hybridization on the MEF effect of F-dsDNA-HMNC conjugates, F-B2A1-S-HMNC3 conjugates were prepared with A1-S (5′ HS-C6-TAC CTGAATGCG 3′)-tagged HNMC3s and one base mismatched F-B2 (5′ FITC-GGCATTCAGGTA 3′) probes. Hybridization was performed in phosphate buffer solutions (0.3 mol $L^{-1}$, pH = 7.0) for 2 h for the three types of DNA hybridization detection. The MEF effects of the prepared F-B2A1-S-HMNC3 conjugates were observed and measured with a fluorescence spectrophotometer.

## 3. Results and discussion

### 3.1. FDTD simulation of the local electric field enhancement around the nanostructures

The enhancement of the local electric field intensity originated from the spatial redistribution of the optical electric field around the metallic nanostructures[37].Electric field redistribution around different nanostructures( AuNPs, AuNP cluster, and AuNPs-$SiO_2$ cluster, and AuNPs-$Fe_3O_4$ cluster ) were simulated via the FDTD method and illustrated in Figs.1 and S1. The excitation

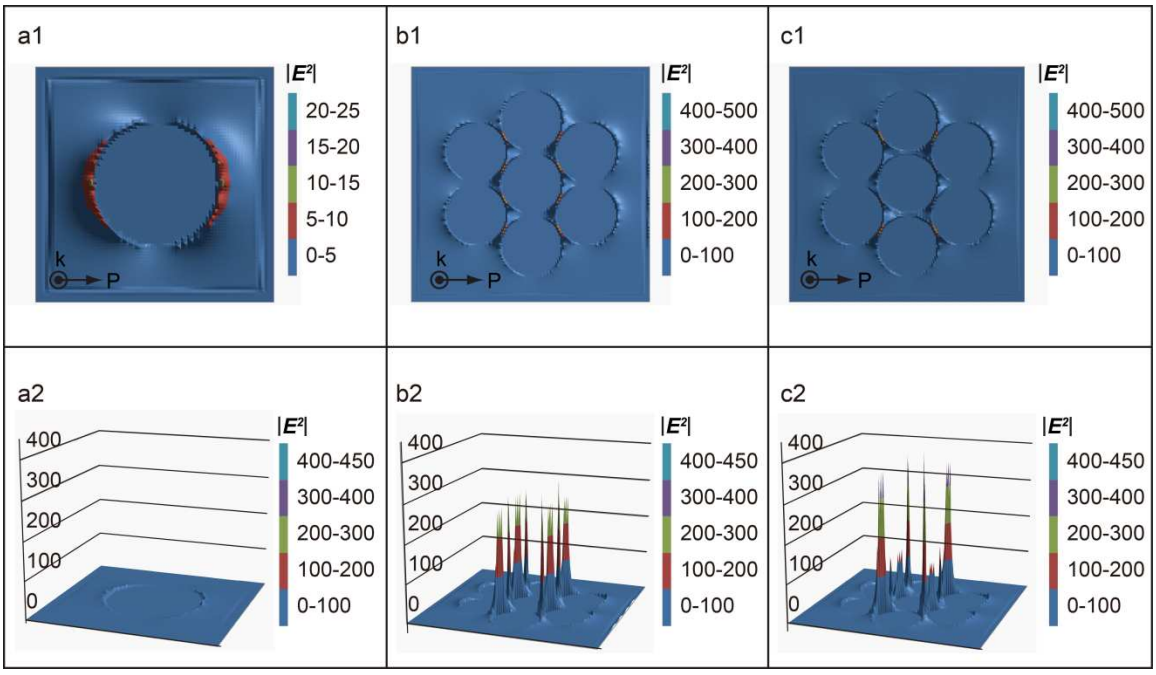


**Fig.1** Finite Difference Time Domain (FDTD) simulation results of the local electric field around different nanostructures. a. Single AuNP (diameter = 20 nm) b. AuNPs cluster consists of 7 AuNPs with gap of 1 nm and c. Au-$Fe_3O_4$ hybrid magnetic NPs cluster (HMNC) consists of 6 AuNPs with gap of 1 nm using $Fe_3O_4$ as the core. Scale bars = 20 nm. The excitation wavelength is 488 nm and incident electromagnetic wave along the z direction is polarized along the symmetry axis and perpendicular to it.

wavelength was 488 nm, and the incident electromagnetic wave along the *z* direction was polarized along the symmetry axis and perpendicular to it. The FDTD simulation results indicate that the maximum local electric field intensity of NP clusters is considerably higher than that of a single AuNP for the coupling effect among the NPs of the cluster [38]. For AuNP cluster, the maximum local electric field intensity was approximately 10-fold than that of a single AuNP. For AuNPs-$SiO_2$ and AuNPs-$Fe_3O_4$ clusters, the enhancements were even higher than those of the other nanostructures (approximately 15-fold of a single AuNP). The "hotspot" (spot with maximum local electric field enhancement) distributions of the HMNCs were also different from those of AuNP cluster. In the case of AuNPs, "hotspots" were positioned at the junctions of both core–satellite and satellite–satellite NPs, whereas in the case of HMNCs, the "hotspots" were only present at the junctions of the satellite–satellites NPs were only present at the junctions of the satellite–satellite NPs. These results indicate that more "hotspots" among NPs can disperse the entire electric field enhancement of the cluster. By contrast, less "hotspots" will enhance the

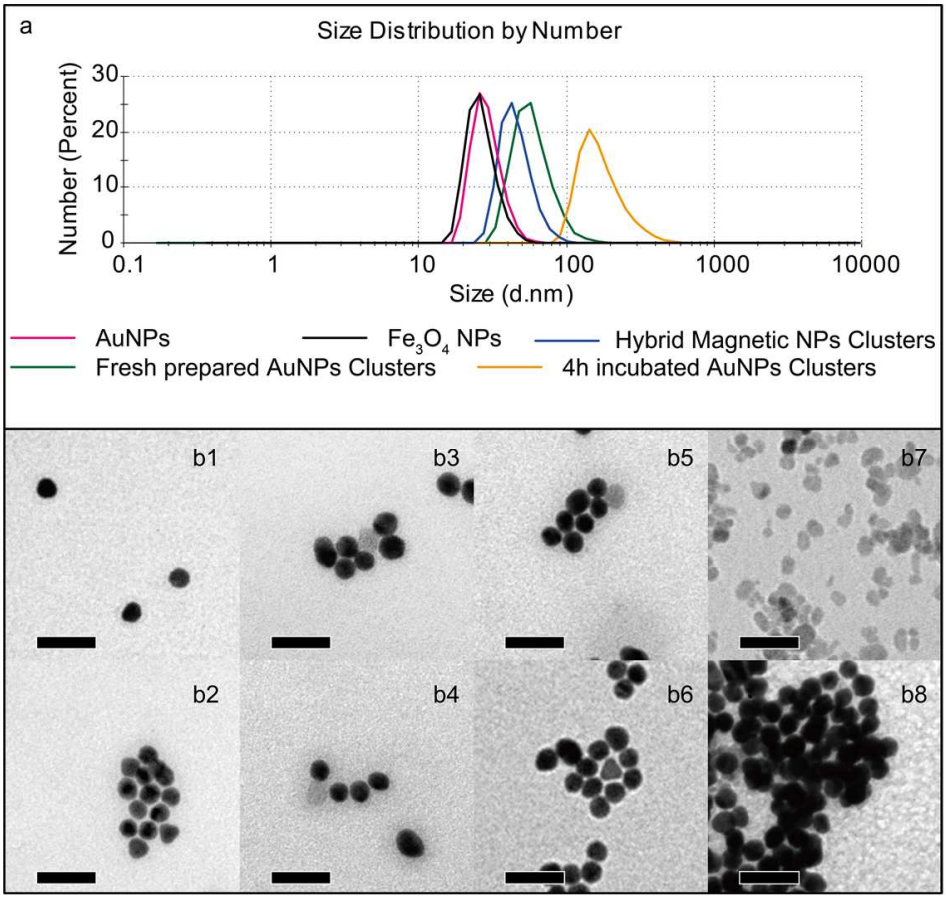


**Fig.2** a. The size distributions of the nanostructures in aqueous media are obtained by dynamic light scattering (DLS): AuNPs (Red), $Fe_3O_4$ NPs (Black), fresh prepared AuNPs clusters (Green), Au-$Fe_3O_4$ hybrid magnetic NPs clusters (HMNC) (Blue) and AuNP clusters after 4 hours (Yellow). b. TEM images of the nanostructures, b1: AuNPs, b2: fresh prepared AuNPs clusters, b3-b6: Au-$Fe_3O_4$ hybrid magnetic NPs clusters (HMNC), which average consist of one $Fe_3O_4$ NP core and about 6 to 8 surrounding AuNPs. b7: $Fe_3O_4$ NPs and b8: AuNP clusters after 4 hours. Scale bars = 50 nm

entire electric field or fluorescence intensity of the cluster. Hybrid AuNP clusters have higher electric field enhancement than AuNP clusters. Both silica and $Fe_3O_4$ NPs demonstrated their effectiveness as core NPs in hybrid magnetic nanoparticle (HMN) assembly. $Fe_3O_4$ NPs have specific advantages. (1) $Fe_3O_4$ NPs and AuNPs were modified with different property of functional groups, thus, $Fe_3O_4$ NPs have a certain number of satellite AuNPs around with them and NP cluster aggregation is not easily occurred. Our previous study established a valid protocol to prepare a stable colloidal solution of $Fe_3O_4$. The surface modification methods of these NPs are also available. (2) We also proved the effectiveness of $Fe_3O_4$ NPs as contrast agents for magnetic resonance imaging (MRI). HMNCs that are composed of one $Fe_3O_4$ NP core and several satellite AuNPs could be used as effective multimode bio-imaging agents with

MRI/computed tomography/MEF imaging effects in further studies[30]. Therefore, we designed a novel hybrid $Fe_3O_4$/AuNP cluster (that is, HMNC) that consists of a certain number of AuNPs around one $Fe_3O_4$ NP. The results showed that these nanostructures are stable in aqueous solutions and that they exhibited higher fluorescence intensity and quantum yields than AuNP cluster.

### 3.2. Size distributions, morphologies, and components of NPs and the prepared nanostructures

To investigate the size and component of these nanoparticles and nanostructures, a series of nanostructures, including AuNPs, AuNP clusters, $Fe_3O_4$ NPs, HMNCs, and DNA-HMNC conjugates, were demonstrated and characterized. The size distributions of these nanostructures in aqueous media are shown in Fig. 2a through the dynamic light scattering (DLS) method. The average diameter of AuNPs (red line) was 22 nm, which is in accordance with the diameter obtained from TEM (19±0.8 nm, Fig. 2b1). The average diameter of fresh prepared AuNP clusters (with 1,6-hexamethylene diamine as a cross-linker, green line) was 97 nm, and then, it increased to 150 nm (yellow line) within 4 h with continuous aggregation. In TEM observations, the average diameter of freshly prepared AuNP clusters was 100±8.1 nm (Fig. 2b2), which is in accordance with the DLS result; however, their aggregates were larger than 200 nm (Fig. 2b8).The DLS results showed that the hydrodynamic diameters of $Fe_3O_4$ NPs and HMNC were 22 nm (black line) and 87 nm (blue line), respectively. DNA-HMNC conjugates have the similar diameters with related HMNCs (data not shown). In addition, $Fe_3O_4$ NP solution was prepared and modified with surface amino groups by treating with the silane coupling agent APTMS. The prepared $Fe_3O_4$@$NH_2$ NPs could be redispersed well in water; the obtained NP solution was transparent and exhibited high stability for several months. The choice of the amino-containing silane coupling agent might affect the colloidal stability of the prepared $Fe_3O_4$@$NH_2$ NPs in water. If APTES was used instead of APTMS, then the prepared $Fe_3O_4$@$NH_2$ NP solution was less transparent and stable. $Fe_3O_4$@$NH_2$ NP solution prepared with APTMS was stable and even maintained its transparency in an applied magnetic field. By contrast, a solution prepared with APTES would be separated in the applied magnetic field in less than 3 min. Given that the $Fe_3O_4$@$NH_2$ NP solution was mixed with the AuNP solution, the positively charged $Fe_3O_4$@$NH_2$ NPs would be aggregated with the negatively charged citrate-stabilized AuNPs, which were assembled into hybrid NP clusters with one $Fe_3O_4$@$NH_2$ NP core and several satellite AuNPs. The amino groups of $Fe_3O_4$ NPs had high affinity toward citrate-stabilized AuNPs, and the assembled hybrid NP clusters exhibited good stability. Furthermore, these assembled hybrid NP clusters did not only demonstrate monodispersity as reported in literature [11], but also retained an unmodified satellite AuNP surface. Besides the amino group, the thiol group also had high affinity toward Au surface. However, the thiol group-modified $Fe_3O_4$@SH NPs were not as stable as $Fe_3O_4$@$NH_2$ NPs in water and would aggregate with one another prior to use, thus limiting their application in HMNC assembly. Figs. 2b8 and 2b3-6 show representative TEM images of the individual $Fe_3O_4$ NPs and HMNCs, respectively. The average diameter of $Fe_3O_4$ NPs was 19±0.8 nm, and the average diameter of the prepared HMNC3 is 87±3.2 nm, which agreed well with the DLS analysis results. In summary, HMNC3 consisted of one $Fe_3O_4$ NP core and an average of six to eight satellite AuNPs, which coincides with the ratio of 1:8 of added $Fe_3O_4$@$NH_2$ NPs to AuNPs.

### 3.3. Colours and UV–vis spectra

Given that AuNPs could aggregate into clusters, the UV–vis spectra of the system would undergo significant changes, and the colour would also change to indicate visual performance [11]. By adding different amounts of $Fe_3O_4$@$NH_2$ NPs into a constant volume of AuNP solution, HMNCs that consisted of different ratios of $Fe_3O_4$@$NH_2$ NPs and AuNPs were prepared.

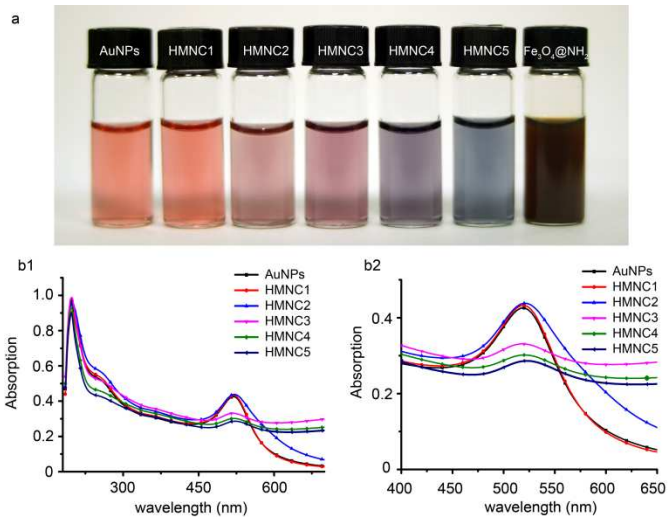


Fig.3 Colours or UV–vis spectra of samples: a. AuNPs, $Fe_3O_4$ @$NH_2$-AuNPs magnetic hybrid NPs clusters (HMNC) of different size and colours; b. UV-vis spectra of the AuNPs and HMNC. HMNC1-5 obtained by adding 0.005, 0.010, 0.015, 0.020 and 0.025 mg $Fe_3O_4$ @$NH_2$ into 4 mL AuNPs solutions (0.096mg $mL^{-1}$).

HMNC1 to HMNC5 with $Fe_3O_4$@$NH_2$ NP to AuNP ratios of approximately 1:24, 1:12, 1:8, 1:6, and 1:5 were prepared by adding $Fe_3O_4$@$NH_2$ NP solution (1.0 mg $mL^{-1}$) of 5, 10, 15, 20, and 25 μL to 4 mL AuNP solution. The result exhibited red, purple, violet, and blue hues (Fig.3a). The optical properties of the HMNCs were further characterized by UV–vis spectroscopy (Fig. 3b). In the absence of $Fe_3O_4$ NPs, the maximum absorption peak of AuNPs was observed at 522 nm. The increase in $Fe_3O_4$ NP amount resulted in the decrease in maximum absorption intensity from 0.43 to 0.29, with significant broadening. This finding agrees well with the colour observation. Changes in the absorption peaks were proportional to the additional quantity of $Fe_3O_4$ NPs (Fig. 3b1). For HMNC1, the intensity and half width of the absorption peaks were both similar to those of Au NPs. For HMNC2, the intensity of the absorption peaks was slightly increased, and the half width of the absorption peaks was slightly broadened. However, a sudden change in the intensity and half width of the absorption peaks was observed with HMNC3, HMNC4, and HMNC5 (Fig. 3b2). The half widths of these three absorption peaks were nearly equally broadened, and the intensities significantly decreased in sequence.

The prepared HMNCs exhibited discernible colours from red to purple and blue, and their absorption spectra had different maximum absorptions. The colour and absorption spectrum of HMNC1 (with $Fe_3O_4$@$NH_2$ NP to AuNP ratio of 1:24) were similar to those of AuNPs, thus indicating that most AuNPs were not assembled as clusters. The colour of HMNC2 remained red, but its absorption spectrum exhibited a number of differences compared with that of AuNPs (with broadened absorption peak). This change in absorption spectrum indicates the formation of NP clusters. Considering that large $Fe_3O_4$@$NH_2$ NP to AuNP ratios were used, the obtained products (HMNC3, HMNC4, and HMNC5) exhibited significantly different characteristics from AuNP solution. The colours of HMNC3, HMNC4, and HMNC5 were deep red, purple, and blue. In addition, a large absorption ranging from 400 nm to 650 nm was exhibited in their absorption spectra. However, the absorption spectra of the prepared HMNCs still exhibited several differences from the reported AuNP clusters. Only one HMNC absorption peak was observed within the range of 400 nm to 650 nm, whereas the absorption spectra of AuNP clusters (which used dithiothreitol as cross-linkers) typically had secondary peaks at long wavelengths [11]. This difference could be attributed to using NPs as cross-linkers instead of small molecules (such as dithiothreitol). Different cross-linkers would lead to a change in the coupling state among AuNPs, as reported in literature [39]. Furthermore, as previously revealed by the FDTD simulation results, the core NPs of the prepared HMNCs were $Fe_3O_4$@$NH_2$ NPs, which were not or only weakly coupled with satellite AuNPs. By contrast, core AuNPs in AuNP clusters were strongly coupled with satellite AuNPs. This difference in coupling modes leads to the differences in absorption spectra.

### 3.4. Stability of the prepared NP clusters and DNA-HMNC conjugations

Studies that used modified NPs as cross-linkers to assemble hybrid NP clusters have been reported [22]; however, studies on the stability of assembled HNCs in solutions are rare. To investigate the stability of the prepared HMNCs and AuNP clusters, UV–vis absorption spectra and hydrodynamic diameter of the prepared samples (HMNC1, HMNC3, HMNC5, and AuNPs clusters) were regularly recorded (every 5 days) after being stored for 1 month because the aggregation of AuNP clusters could lead to changes in their absorption spectra. Fig. 4a showed that the maximum absorption of the prepared AuNP clusters drastically declined in 5 days and significantly decreased in 30 days. This trend indicates their continuous aggregation in a solution. The maximum absorption of the prepared HMNC5 was also decreased to less than 0.4 during storage. By contrast, the maximum absorptions of the prepared HMNC1 and HMNC3 solutions were basically constant in 15 days and only slightly decreased in 30 days, thus indicating their good stability in solutions. The same results can be found in hydrodynamic diameter detection (data not shown). The prepared HMNC3s were conjugated with alkanethiol-terminated ssDNA molecules. Notably, the addition of these molecules was approximately 1/10 of those in the work of Mirkin *et al* [33], which was attributed to their protocols. High surface conjugation density was obtained by using NaCl and sodium dodecylsulfate (SDS) solution. The use of SDS in our system would lead to aggregation of the prepared HMNCs. The reason for such aggregation requires further investigation.

Successful conjugation of the alkanethiol-terminated ssDNA molecules on the surface of the prepared HMNC was confirmed by testing the colloidal stability of DNA-HMNC conjugations in NaCl solution with different concentrations. As reported in literature [40,41], DNA conjugated AuNPs exhibited high stability in solutions with high ionic strength. Thus, if the surface of the prepared HMNCs was successfully conjugated with DNA molecules, then better resistance

to such solutions would be demonstrated compared with those of their unmodified counterparts. The prepared DNA-NPs, DNA-HMNC conjugates, and their unmodified counterparts were dispersed in deionized water, 0.15 mol $L^{-1}$ NaCl solution, and 1.0 mol $L^{-1}$ NaCl solution, respectively. Then, their UV–vis spectra were recorded. As shown in Fig. 4b, except for HMNC5, the absorption peaks of DNA-HMNC1, DNA-HMNC3, and DNA-AuNP conjugates remained nearly unchanged in deionized water and 0.15 mol $L^{-1}$ NaCl solution. This result indicates successful conjugation of the ssDNA molecules. In 1.0 mol $L^{-1}$ of NaCl solution, the maximum absorption intensity of the four NP conjugates sharply declined. For their unmodified counterparts,

**Table.1.** Fluorescent intensity between fluorophores and nanostructured metal surfaces or adsorbed colloidal particles

| Substrate | Fluorophore | Maximum enhancement | Ref |
|---|---|---|---|
| Silver Island film | Fluorescein-labeled immunoglobulin G (Fl-IgG) | 40 | 45 |
| Silver Island film | Fluorescein-labeled 23-mer Oligo | 2.5 | 46 |
| AuNPs | Fluorescein isothiocyanate-human serum albumin (FITC-HSA) | 11.8 | 47 |
| Au NPs with MS2 Viral Capsids | AF488-dsDNA | 2.2 | 48 |
| Au NPs@$SiO_2$ | TAMRA-SE | 9.2 | 49 |
| Magnetic Hybrid NPs cluster conjugate (HMNC) | FITC-dsDNA | 10.8 | |

poor stability was observed in similar NaCl solution A than their unmodified counterparts. In addition, thiol-containing molecules can interact with metal ions and metal surfaces to form dative bonds[42]. Alkanethiol capped oligonucleotides have been widely used in the modification and bio-conjugation of gold thin films and AuNPs. Surface conjugation of alkanethiol capped DNA probes on gold thin film can be characterized by a number of techniques, including electrochemistry, XPS, and surface plasmon resonance spectroscopy[43]. However, due to the small size of AuNPs, conjugation of oligonucleotides on the surface of AuNPs is not easy to characterize by common methods. Citrate-stabilized AuNPs exhibit very poor electrostatic stability and may form aggregates when just small quantities of salt are added (about 10 mmol $L^{-1}$)[44], and surface conjunction of hydrophilic DNA molecules can greatly enhance the stability of AuNPs in solution containing salt. Thus, investigation of the colloidal stability of the modified AuNPs in salt solutions is an easy and effective method to affirm the successful conjugation of DNA molecules on AuNPs surfaces.

We further investigated the effect of pH (Fig. 5b) and temperature (Fig. 5c) on F-B1A1-S-HMNC3 conjugates. The results showed that the enhancement factor slightly changed in pH 3.0 to pH 8.0 and within the temperature range of 25 °C to 50 °C. Thus, the aforementioned HMNCs can be used as effective MEF substrates under such conditions.

### 3.5. Hybridization efficiency and self-absorbance effects of DNA-HMNC conjugations

To measure quantitatively the efficiency of DNA probe hybridization efficiency, different equivalents of F-B1 solutions, with varying quantities ranging from 0.1 to 1.0 (0.10 interval), were added into the prepared HMNC solutions to form F-B1A1-S-HMNC3 conjugates. The fluorescence intensities (at 525 nm) of the prepared conjugates were recorded (Fig. 4c). The addition of cDNA resulted in increased fluorescence intensity. Maximum fluorescence intensity was achieved with equivalents of 0.8, thus indicating maximum hybridization efficiency of approximately 80%. It is also confirmed that most of the added alkanethiol-terminated ssDNA molecules were successfully conjugated onto the surface of HMNCs (Fig. 4c).The effects of self-absorbance on the recorded fluorescence spectra were also studied. Thus, the prepared F-B1A1-S-HMNC3 conjugates were exponentially diluted (1-, 2-, 4-, 8-, and 16-fold), and fluorescence intensities (at 525 nm) were recorded (Fig. 4d). Compared with the theoretical value curve (which decreased exponentially from the fluorescence intensity of the undiluted sample without considering self-absorbance), the intensity of the experimental value was higher (106%) after 4-fold dilution. This difference could be attributed to the occurrence of self-absorption. Therefore, given that fluorescence spectra were recorded with diluted solutions, the self-absorption effect was lower and its influence toward further experiments was tolerable.



 

However, "Salt solution test" can only qualitatively determine the results of the conjugation process, investigation of the quantified details, such as surface coverage and conjugation rate, relies on further experiments. According to the method reported by L. M. Demer with some modification[33], we designed an experiment to measure the surface coverage and conjugation rate of DNA molecules on the prepared HMNCs. The measured results showed that about 20 nmol DNA probes could be conjugated with every 5 mL of the prepared HMNCs.

### 3.6. The MEF effect of F-B1A1-S-HMNC3 conjugates in solutions

The MEF effect of ssDNA-S-HMNC conjugates could be characterized by two indices, namely, fluorescence intensity (maximum or at a certain wavelength) and enhancement factors. Fluorescence spectra obtained from HMNCs of different Au/$Fe_3O_4$ NP ratios are shown in Fig. 5a. Compared with F-ssDNA, various HMNC exhibited different MEF effects. The fluorescence intensities of F-B1A1-S-HMNC1 conjugates and F-B1A1-S-HMNC2 conjugates both slightly decreased, whereas those of F-B1A1-S-HMNC1 conjugates 3, F-B1A1-S-HMNC1 conjugates 4, and F-B1A1-S-HMNC5 conjugates all significantly increased, particularly as shown in Fig. 5d. Compared with the reported enhancement factors obtained from various MEF substrates (planar substrates/in solution) with a fluorophore and an analogous quantum yield, an enhancement factor of 10.8 was higher, as shown in Table 1 [47–51]. Given that the enhancement factor is not only associated with the substrate, but also with the initial quantum yield of the fluorophore used, high enhancement factors may be obtained by using a fluorophore with low initial quantum yield, such as crystal violet [21]. The influence of the surrounding pH values on the fluorescence enhancement factor was investigated. Fig.5b showed the histogram of the obtained fluorescence enhancement factor versus pH value. From pH 3.0 to pH 8.0, the fluorescence enhancement factor was always above 6, thus indicating that the system could be used in a wide range of pH values. The fluorescence enhancement factor reached a maximum of 11.0 at pH 7.0. This result indicates that the system is especially suitable at pH 7.0, which is close to the physiological pH value. Subsequently, the effects of temperature were investigated. As showed in Fig. 5c, the fluorescence enhancement factor of the F-B1A1-S-HMNC conjugates varies at different temperatures (25 °C to 50 °C). At temperatures lower than calculated *T*m (46.3 ºC), the F-B1A1-S-HMNC conjugates show high fluorescence enhancement of 11.1 (at 25 ºC), 10.7 (at 30 ºC), 10.9 (at 35 ºC), and 9.4 (at 40 ºC). At temperatures near or higher than the calculated *T*m, the fluorescence intensity of the conjugates drastically decreased, the enhancement factors drop to 3.4 (at 45 ºC) and 0.9 (at 50 ºC). This phenomenon can be explained as follows: the F-B1A1-S-HMNC3 conjugates, which possessed a 10.8 fold maximum enhancement factor. Notably, the enhancement factors of these conjugates remained nearly unchanged in 1 month (recorded every 5 days).

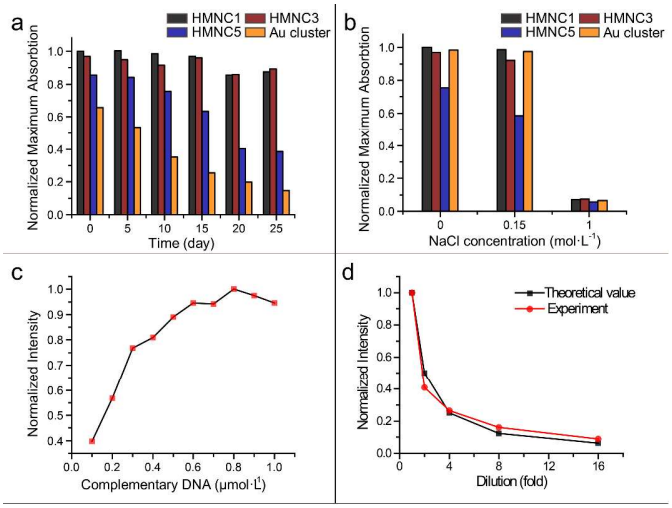


Fig.4 a. Normalized maximum absorption of Au cluster and three different magnetic hybrid conjugates (HMNC1, HMNC3 and HMNC5) stored for periods of time (0-30 days);b. Normalized maximum absorption of DNA-MHNC1, DNA-HMNC3 and DNA-HMNC5 conjugates in NaCl solutions of three different concentrations (0, 0.15 mol $L^{-1}$, 1mol $L^{-1}$) respectively; c. Fluorescence intensity of F-B1A1-S-HMNC3 conjugates formed with F-B1 solutions of different concentrations (0.01-0.1 μmol $L^{-1}$); d. Fluorescence intensity of 0.08μmol $L^{-1}$ F-B1 solutions formed with F-B1A1-S-HMNC3 conjugates of different concentrations by exponential diluted.

**Table 2** Fluorescence Intensity Decay Analysis

| | τ1(ns) | Amplitude | τ2(ns) | Amplitude | τ3(ns) | Amplitude | τave.(ns) |
|---|---|---|---|---|---|---|---|
| F-B1 | 1.328 | 0.012 | 3.826 | 0.988 | N/A | N/A | 3.797 |
| F-B1A1-AuNPs | 0.433 | 0.051 | 1.741 | 0.670 | 2.990 | 0.280 | 2.024 |
| F-B1A1-HMNCs | 0.172 | 0.255 | 1.344 | 0.726 | 3.021 | 0.019 | 1.077 |

[a] Footnote τ1, τ2, τ3 denotes decay times of the three lifetime components, and $\tau_{ave}$ is the average lifetime

enhancement factor of the conjugates is strongly influenced by the hybridization between the fluorescein tagged F-B1 DNA and the A1-S DNA conjugated HMNCs. As the surrounding temperature reaches the *T*m of the F-B1 and A1-S DNA pair, the melting of F-B1A1-S dsDNA will lead to dissociation of the F-B1 from the conjugates, thus leads to the absent of MEF effects and gives a lower enhancement factor. Besides the length, the specific nucleotide sequence of the DNA molecules and the salt concentration of the buffer solution used, the *T*m of

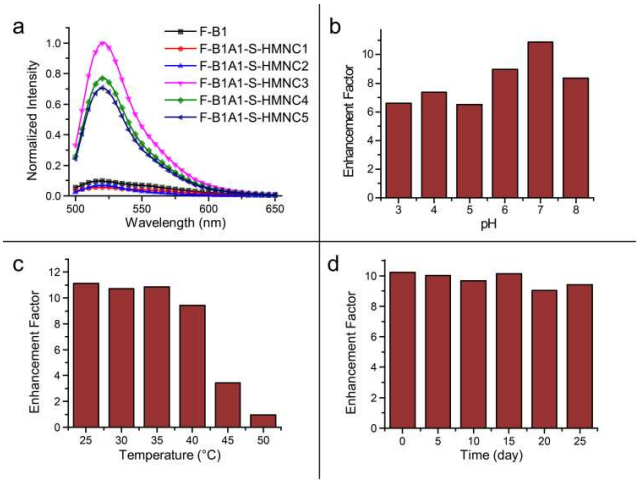


Fig. 5 a. Fluorescence spectra of F-B1A1-S-HMNC conjugates formed with HMNC of different Au/$Fe_3O_4$ NPs ratios; b. Fluorescence enhancement factors of F-B1A1-S-HMNC3 conjugates in solutions of different pH values; c. Fluorescence enhancement factors of F-B1A1-S-HMNC3 conjugates at different temperatures (25-50°C); d. Fluorescence enhancement factors of F-B1A1-S-HMNC3 conjugates stored for periods of time (0-30 days).

the dsDNA is also influenced by the pH of the solution[50]. D. Yu. Lando *et.al.,* reported their study on the prediction of Tm with different solution pH in 1994[51]. However, common *T*m calculation software does not provide *T*m prediction function with variable solution pH values. To determine the influence of pH to the *T*m of the DNA probe we used, we have roughly measured the *T*m of the DNA probe we used with pH 3.0 of buffer solution, pH 4 of buffer solution and pH 7.0 of PBS buffer solution. The measured *T*m were 28 ºC (pH 3.0), 44 ºC (pH 4.0) and 47 ºC (pH 7.0 PBS), respectively. The obtained *T*m decreased about 36% as the pH values changed from 7.0 to 3.0. This trend is partiality coincide with the study reported by M.C.Williams *et.al* [52]., in which the *T*m of the dsDNA (with buffer solution containing 250 $mmol^{-1}$ NaCl ) decreased from 81.4 ºC to 48.8 ºC (a decrease of 40%), as the pH value of the buffer solution changed from 9.2 to 3.1. However, it is need to point out, as *Tm* of the dsDNA is influenced by solution pH, the pH of the buffer solution used should be properly confined in the range of 5.0 to 9.0.

3.7. Fluorescence spectra of F-B1A1-S-HMNC3 conjugates

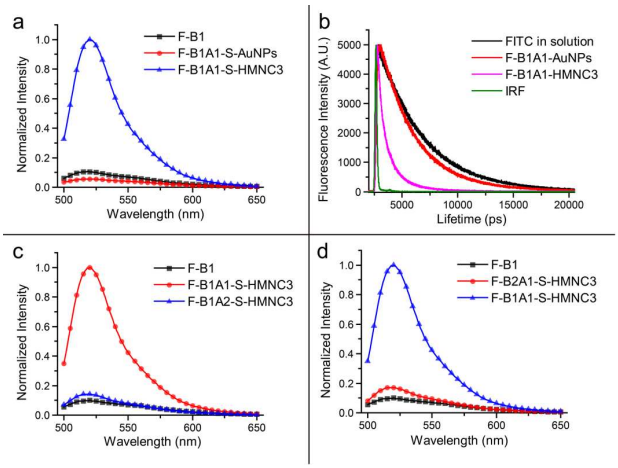


**Fig.6** Fluorescence spectra of F-dsDNA conjugates formed with different NPs or NP clusters; a. F-B1A1-S-HMNC3 conjugates, F-B1 solution and F-B1A1-S-AuNPs conjugates; b. Representative fluorescence lifetime decay curves. From top to bottom: F-B1 solution, F-B1A1-S-AuNP conjugates, F-B1A1-S-HMNC3 conjugates and reference; c. Fluorescence spectra of F-B1A1-S-HMNC3 conjugates (with 5'-labeled complementary DNA) conjugates, F-B1A2-S-HMNC3 conjugates (with 3'-labeled complementary DNA) conjugates and F-B1 solution; d. Fluorescence spectra of F-B1A1-S-HMNC3 conjugates (with 5'-labeled), F-B2A1-S-HMNC3 (with 5'-labeled mismatch DNA) conjugates and F-B1 solution.

To assess the effects of different NPs or NP clusters on fluorescence enhancement, we conducted model hybridization with a complementary F-ssDNA. The experiment was designed to ensure that F-ssDNA and its complementary alkanethiol ssDNA-modified surfaces of different NPs or NP clusters under hybridization conditions were accurately corrected. Figs. 5a and 6a showed that the fluorescence intensity of F-B1A1-S-HMNC3 conjugates was notably higher than those of the others. We emphasized that the emission spectra shapes of F-B1, F-B1A1-S-AuNPs, and F-B1A1-S-HMNC3 conjugates were similar, and that their maximum wavelengths were 518, 518, and 519 nm, respectively. Their normalized intensities were 0.1069, 0.0559, and 1.0, respectively. These results indicate that HMNC3 can remarkably enhance the fluorescence intensity of F-B1 under hybridization conditions. These results indicate that HMNC3 can remarkably enhance the fluorescence intensity of F-B1 under hybridization conditions. By contrast, AuNPs slightly decreased the fluorescence intensity of F-B1. As discussed in literature [53], MEF is accompanied by an increase

Nanoscale RSCPublishing

ARTICLE

in quantum yield and a decrease in the lifetime of a fluorophore located within the proximity of metallic nanoparticles.The fluorescence lifetime provided an unambiguous distinction of the metal-induced fluorescence enhancement. To confirm the enhancement mechanism, the representative lifetimes of F-B1 solution, F-B1A1-S-AuNP conjugates, F-B1A1-S-HMNC3 conjugates, and a reference were measured under the same experimental conditions.

The stronger metal-enhanced fluorescence effect showed by HMNC3 was originated from its well assembled core-satellite nanostructure. Compare with single AuNP, aggregation of the clustered satellite AuNPs produce higher enhanced local electric field, which could be seen from the FDTD simulation comparison of these two kinds of nanostructures. In other HMNCs prepared with less $Fe_3O_4$ NPs core addition, such as HMNC1 and HMNC2, the core-satellite nanostructures are less well assembled, and their UV-vis absorption spectra present similar characteristics than that of the AuNPs. In HMNCs prepared with more $Fe_3O_4$ NPs core addition, such as HMNC4 and HMNC5, more than one cores have been incorporated into the NPs cluster assemblies. Compare with HMNC3, these HMNCs have red-shifted decreased absorption spectra, and their MEF effects are found weaker than HMNC3 (Fig.3a). As MEF effect is originated and mainly influenced by the local electric field enhancement effect of the nanostructures, decrease in MEF effect can be attributed to the featured plasmonic coupling states of these nanostructures. an even define explanation of this phenomena needs further studies in the electric field enhancement effect of nanostructures with multiple cores, and which is relied on more FDTD simulation results (have the miscellaneous nanostructures been well simulated). We are now working on the relative studies and further results will be reported in our later works.

The decay curves in Fig. 6b showed a significant reduction in the fluorescence lifetime of F-B1A1-S-HMNC3 conjugates compared with those of F-B1 solution and F-B1A1-S-AuNP conjugates. Table 2 showed their values and the average lifetimes of different samples. For F-B1A1-S-HMNC3 conjugates, the obtained average lifetime was approximately 1.077 ns. For the remaining samples, the obtained average lifetimes of FITC solutions and F-B1A1-S-AuNP conjugates were 3.797 and 2.024, respectively. These reduced lifetimes were attributed to the interaction of the excited fluorophores with surface plasmon resonances in metals, which is particularly prominent in metal nanostructures [54]. These effects had two major implications: high photostability and a high amount of emitted photons per unit time under the same excitation conditions. Both of these properties enable the use of short exposure time or attaining high signal-to-noise ratio for comparable exposure times, thus increasing sensitivity to and selectivity in fluorescence measurements.

### 3.8. DNA hybridization detection

The mechanism of MEF is complex, as illustrated by recent theoretical and experimental studies[18]. Various reports have experimentally demonstrated MEF, but the design principles to achieve maximum fluorescence enhancement remain unclear. Systematically addressing various factors that influence the magnitude of MEF is critical in designing ultrasensitive fluorescence probes. In contrast to the study of Gill *et al* [23] who used AgNP cluster as MEF substrate in solutions, in which F-DNA molecules were directly absorbed on the surface of AgNP clusters, the MEF effect of the HMNCs prepared in the present study could be associated with distance. As Table S1 shown, the prepared F-D1C1-S-HMNCs conjugates (with fluorophore-nanostructure distance of about 5nm) possess MEF enhancement factor of about 8, while the F-D2C1-S-HMNCs conjugates (with fluorophore-nanostructure distance of about 3nm) possess enhancement factor of about 2, and the F-D3C1-S-HMNCs conjugates (in which the inter-distance are quite short) possess enhancement factor of about 1. While F-B1A1-S-HMNC conjugates possesses fluorescence emission about 10 times higher than that of the solution of F-B1 DNA probe, while fluorescence emission of the F-B1A2-S-HMNC conjugates is only slightly higher than that of the F-B1 solution. These results showed distance-dependent MEF effect of this study has been existed. The suitable distance of MEF effect in this study is about 4nm.

The specificity of the novel method was also investigated by using a fully complementary ssDNA and a single-base mismatched ssDNA. Fig. 6d showed that the signal from the single-base mismatched ssDNA was approximately 17.0% of the signal from the fully complementary 12 mer sequence after 2 h. This result coincides with that reported in literature[55] (compared with that from the fully complementary sequence, the same signal from the four-base mismatched 23 mer ssDNA was slower). DNA-modified HMNCs in our work exhibited significant distance-dependent MEF effect after DNA hybridization. A single mismatch exactly matches the intensity of only 17.0%, thus suggesting that this novel DNA detection method is highly specific and can be used to differentiate even a single-base mismatch. Based on the aforementioned results, the previously mentioned MEF substrate (HMNCs) can be used as a nanosensor for DNA hybridization, which is in contrast with the result of literature [23]. As confirmed in our previous study [30], $Fe_3O_4$ NPs used in HMNC assembly are effective T2 MRI contrast agent. The prepared HMNCs can also be used as an MRI/MEF dual-functional nanosensor for bio-imaging and sensing.

## 4. Conclusions

We designed and prepared a novel hybrid magnetic Au/$Fe_3O_4$ nanocluster (HMNC) by using the amino group-modified $Fe_3O_4$NP either as the core or as cross-linkers. These nanostructures control six to eight satellite AuNPs surrounding a single $Fe_3O_4$NP core. Fluorescein isothiocyanate tagged DNA-HMNC is stable in aqueous solutions and exhibits significant distance-dependent MEF effect and high specificity after DNA hybridization. This result indicates that DNA-HMNC can be extensively used in sensor and biomedical field applications.

## Acknowledgements

This study was supported in part by National Basic Research Program 973 of China (No.2010CB732603 and No.2011CB707903), the National Nature Science Foundation of China (Nos. 81271686 and 81228011), and the grants of Shaanxi province science and technology and innovation project (Nos. 2011KTCL03-07).

## Notes and references

[a] *Key Laboratory of Biomedical Information Engineering of the Education of Ministry, School of Life Science and Technology, Xi'an Jiaotong University, Xi'an, 710049, P. R. China*

[b] *College of Chemistry and Chemical Engineering, Xi'an Shiyou University, Xi'an 710065, P. R. China*

† *These authors contributed equally to this study.*

* *Correspondence author should be addressed. E-mail: wudaocheng @ mail.xjtu.edu.cn; Tel: +86 2982663941*

Electronic Supplementary Information (ESI) available: Fig.S1-Fig.S2, See DOI: 10.1039/b000000x/

1 M. R. Jones, K. D. Osberg, R. J. Macfarlane, M. R. Langille and C. A. Mirkin, *Chem. Rev.* 2011, **111**, 3736-3827.
2 M. E. Stewart, C. R. Anderton, L. B. Thompson, J. Maria, S. K. Gray, J. A. Rogers and R. G. Nuzzo, *Chem. Rev*., 2008, **108**, 494-521.
3 D. A. Giljohann, D. S. Seferos, W. L. Daniel, M. D. Massich, P. C. Patel and C. A. Mirkin, *Angew. Chem.*, 2009, **121**, 870-885; *Angew. Chem. Int. Ed*., 2009, **48**, 856-870.
4 K. Saha, S. S. Agasti, C. Kim, X. N. Li and V. M. Rotello, *Chem. Rev.* 2012, **112**, 2739-2779.
5 W. Pan, T. T. Zhang, H. J. Yang, W. Diao, N. Li and B. Tang, *Anal. Chem.*, 2013, **85**, 10581-10588.
6 K. M. Wang, Z. W. Tang, C. Y. J. Yang, Y. M. Kim, X. H. Fang, W. Li, Y. R. Wu, C.D. Medley, Z. H. Cao, J. Li, P. Colon, H. Lin and W. H. Tan, *Angew. Chem. Int. Ed*., 2009, **48**, 856-870.
7 N. Geertsa and E. Eiser, *Soft Matter*, 2010, **6**, 4647-4660.
8 J. Zheng, G. Z. Zhu, Y. H. Li, C. M. Li, M. X. You, T. Chen, E. Q. Song, R. H. Yang and W. H. Tan. *ACS Nano*, 2013, **7**, 6545-6554.
9 S. J. Tan, M. J. Campolongo, D. Luo and W. L Cheng, *Nat. Nanotech*, 2011, **6**, 268-276.
10 G. K. Darbha, A. Ray and P. C. Ray, *ACS Nano*, 2007, **1**, 208-214..
11 J. Y. Kim and J. S. Lee, *Nano. Lett.*, 2009, **9**, 4564-4569.
12 S. Shimron, A. Cecconello, C. H. Lu and I. Willner, *Nano Lett*., dx.doi.org/10.1021/nl4017539.
13 J. R. Lakowicz. Plasmonics, 2006, **1**, 5-33.
14 H. Li, M. Wang, C. Z. Wang, W. Li, W.B. Qiang and D. K. Xu, *Anal. Chem.,* 2013, **85**, 4492-4499.
15 J. Zhang, Y. Fu and J. R. Lakowicz, *J. Phys. Chem. C*, 2007, **111**, 50-56.
16 G. P. Acuna, F. M. Möller, P. Holzmeister, S. Beater, B. Lalkens and P. Tinnefeld, *Science*, 2012, **338**, 506-510.
17 N. J. Halas, S. Lal, W. S. Chang, S. Link and P. Nordlander, *Chem. Rev.* 2011, **111**, 3913-3961.
18 D. Darvill, A. Centeno and F. Xie, *Phys. Chem. Chem. Phys*., 2013, **15**, 15709-15726.
19 J. Chen, Y. H. Jin, N. Fahruddin and J. X. J. Zhao, *Langmuir*, 2013, **29**, 1584-1591.
20 S. L. Capehart, M. P. Coyle, J. E. Glasgow and M. B. Francis, *J. Am. Chem. Soc*., 2013, **135**, 3011-3016.
21 H. F. Yuan, S. Khatua, P. Zijlstra, M. Yorulmaz and M. Orrit, *Angew. Chem.*, 2013, **125**, 1255-1259; *Angew. Chem. Int. Ed*., 2013, **52**, 1217-1221.
22 C. Schmidtke, H. Kloust, N. G. Bast´us, J. P. Merkl, H. Tran, S. Flessau, A. Feld, T. Schottenb and H. Weller, *Nanoscale*, 2013, **5**, 11783-11794.
23 R. Gill and E. C. Le Ru, *Phys. Chem. Chem. Phys.*, 2011, **13**, 16366-16372.
24 C. A. Mirkin, R. L. Letsinger, R. C. Mucic and J. J. Storhoff, *Nature*, 1996, **382**, 607-609.
25 B. Tinland, A. Pluen, J. Sturm and G. Weill, *Macromolecules,* 1997, **30**, 5763-5765.
26 J. J. Storhoff, R. Elghanian, C. A. Mirkin and R. L. Letsinger, *Langmuir*, 2002, **18**, 6666-6670.



 

27 W. J. Parak, T. Pellegrino, C. M. Micheel, D. Gerion, S. C. Williams and A. P. Alivisatos, *Nano Lett*., 2003, **3**, 33-36.
28 S.K. Sivaraman, S. Kumar and V. Santhanam, *J. Colloid Interface Sci.*, 2011, **361**, 543-547.
29 J. Hu, L. Wang, F. Li, Y. L. Han, M. Lin, T. J. Lu and F. Xu, *Lab Chip,* 2013, **13**, 4352-4357.
30 Y. Li, Y. S. Wu, C. Luo, F.L Yang, L. Qin, Tao F, G.Q. Wei, X.W.Kang and D. C. Wu, *J. Mater. Chem. B*, 2013, **1**, 4644-4654.
31 K. Aslan, M. J.R. Previte, Y. X. Zhang and C. D. Geddes. *J. Phys. Chem. C*, 2008, **112**, 18368-18375.
32 N. L. Rosi, D. A. Giljohann, C. S. Thaxton, A. K. R. Lytton-Jean, M. S. Han and C. A. Mirkin, *Science*, 2006, **312**, 1027-1030.
33 L. M. Demers, C. A. Mirkin, R. C. Mucic, R. A. Reynolds, R. L. Letsinger, R. Elghanian and G. Viswanadham, *Anal. Chem.*, 2000, **72**, 5535-5541
34 C. Schildkraut and S. Lifson, *Biopolymers*, 1965, **3**, 195-208.
35 W. Rychlik, W. J. Spencer and R. E. Rhoads, *Nucleic Acids Research*, 1990, **18**, 6409-6412.
36 Z. X. Wang, B. E. Tan, I. Hussain, N. Schaeffer, M. F. Wyatt, M. Brust and A. I. Cooper, *Langmuir*, 2007, **23**, 885-895.
37 M. Svedendahl, S. Chen and M. Käll. Nanoplasmonic Sensors, Springer Science+Business Media, New York, America, 2012, 210-371.
38 S. K. Ghosh and T. Pal, *Chem. Rev.*, 2007, **107**, 4797-4862.
39 J.W. Park and J. S. Shumaker-Parry, *J. Am. Chem. Soc.*, 2013, doi.org/10.1021/ja4097384.
40 R. Levy, Z. X.Wang, L. Duchesne, R. C. Doty, A. I. Cooper, M. Brust, D. G. Fernig, *Chem. Bio. Chem.*, 2006, **7**, 592-594.
41 D. K. Lim, Mi. H. Cui and J. M. Nam, *J. Mater. Chem*., 2011, **21**, 9467- 9470.
42 G. T. Hermanson. Bioconjugate Techniques (2nd Edition), Elsevier Inc., London, UK, 2008, 50-100.
43 C. S. S. R. Kumar. Biofunctionalization of Nanomaterials, WILEY-VCH Verlag GmbH & Co. KGaA, Weinheim, Germany, 2005, 99-120
44 J. R. Lakowicz, C. D. Geddes, I. Gryczynski, J. Malicka, Z. Gryczynski, K. Asian, J. Lukomska, E. Matveeva, J. A. Zhang, R. Badugu and J. Huang, *J. Fluoresc.*, 2004, **14**, 425-441.
45 K. Asian, S. N. Malyn, G. Bector and C. D. Geddes, *Analyst*, 2007, 132, 1122-1129.
46 F. Xie, M. S. Baker and E. M. Goldys, *Chem. Mater.,* 2008, **20**, 1788-1797.
47 S. L. Capehart, M. P. Coyle, J. Glasgow and M. B. Francis. *J. Am. Chem. Soc.*, 2013, **135**, 3011-3016.
48 J. Chen, Y. H. Jin, N. Fahruddin and J. X. J. Zhao, *Langmuir*, 2013, **29**, 1584-1591.
49 P.O.P. Ts'o, G. K. Helmkamp and C. Sander, *Proc. Natl. Acad. Sci. USA*, 1962, **48**, 686-697
50 D.Y. Lando, S. G. Haroutiunian, A. M. Kul'ba, E. B. Dalian, P. Orioli, S. Mangani and A. A. Akhrem, *J. Biomol. Struct. Dyn.*, 1994, **12**, 355-366
51 M.C.Williams, J. R. Wenner, I. Rouzina and V. A. Bloomfield, *Biophys J*, 2001, **80**, 874-881
52 W. Deng, K. Drozdowicz-Tomsia, D. Y. Jin and E. M. Goldys, *Anal. Chem*., 2009, **81**, 7248-7255.
53 J. R. Lakowicz, K. Ray, M. Chowdhury, H. Szmacinski, Y. Fu, J. Zhang and K. Nowaczyk, *Analyst*, 2008, **133**, 1308-1346.
54 L. Touahira, E. Galopinb, R. Boukherroub, A. C. Gouget-Laemmela, J. N. Chazalviela, F. Ozanama and S. Szunerits. Biosens. Bioelectron., 2010, **25**, 2579-2585.